Journal of Experimental Botany, Vol. 61, No. 14, pp. 4109–4122, 2010
doi:10.1093/jxb/erq226 Advance Access publication 6 August, 2010
This paper is available online free of all access charges (see http://jxb.oxfordjournals.org/open_access.html for further details)

Journal of Experimental Botany
www.jxb.oxfordjournals.org

RESEARCH PAPER

Growth of the C_4 dicot *Flaveria bidentis*: photosynthetic acclimation to low light through shifts in leaf anatomy and biochemistry

Jasper J. L. Pengelly[1,*], Xavier R. R. Sirault[2], Youshi Tazoe[1,3], John R. Evans[1], Robert T. Furbank[2] and Susanne von Caemmerer[1]

[1] Research School of Biology, The Australian National University, Canberra, Australia
[2] High Resolution Plant Phenomics Centre, CSIRO Plant Industry, Canberra
[3] Graduate School of Biostudies, Kyoto University, Sakyo, Kyoto, Japan

* To whom correspondence should be addressed. E-mail: jasper.pengelly@anu.edu.au

Received 19 May 2010; Revised 19 May 2010; Accepted 28 June 2010

Abstract

In C_4 plants, acclimation to growth at low irradiance by means of anatomical and biochemical changes to leaf tissue is considered to be limited by the need for a close interaction and coordination between bundle sheath and mesophyll cells. Here differences in relative growth rate (RGR), gas exchange, carbon isotope discrimination, photosynthetic enzyme activity, and leaf anatomy in the C_4 dicot *Flaveria bidentis* grown at a low (LI; 150 μmol quanta m^2 s^{-1}) and medium (MI; 500 μmol quanta m^2 s^{-1}) irradiance and with a 12 h photoperiod over 36 d were examined. RGRs measured using a 3D non-destructive imaging technique were consistently higher in MI plants. Rates of CO_2 assimilation per leaf area measured at 1500 μmmol quanta m^2 s^{-1} were higher for MI than LI plants but did not differ on a mass basis. LI plants had lower Rubisco and phospho*enol*pyruvate carboxylase activities and chlorophyll content on a leaf area basis. Bundle sheath leakiness of CO_2 (ϕ) calculated from real-time carbon isotope discrimination was similar for MI and LI plants at high irradiance. ϕ increased at lower irradiances, but more so in MI plants, reflecting acclimation to low growth irradiance. Leaf thickness and vein density were greater in MI plants, and mesophyll surface area exposed to intercellular airspace (S_m) and bundle sheath surface area per unit leaf area (S_b) measured from leaf cross-sections were also both significantly greater in MI compared with LI leaves. Both mesophyll and bundle sheath conductance to CO_2 diffusion were greater in MI compared with LI plants. Despite being a C_4 species, *F. bidentis* is very plastic with respect to growth irradiance.

Key words: C_4 photosynthesis, carbon isotope discrimination, CO_2 leakiness, *Flaveria bidentis*, gas exchange, image analysis, leaf anatomy.

Introduction

As light is a fundamental requirement for photosynthesis, growing plants in a light-limiting environment can affect the development and physiology of leaves. In C_3 species these adaptive changes have been well documented and can include structural, biochemical, and physiological modifications to leaves. At low irradiance, C_3 plants tend to allocate less energy to root production and direct it instead to increase leaf and stem biomass (Poorter and Perez-Soba, 2001). Changes in the size, shape, and number of leaf mesophyll cells reduce leaf thickness and increase specific leaf area (SLA; the leaf area to leaf dry mass ratio), acting to maximize light absorption and reduce the diffusion pathway of CO_2 to photosynthetic tissue (Bjorkman, 1981). The amount of the essential CO_2-fixing enzyme ribulose-1,5-bisphosphate carboxylase/oxygenase (Rubisco) decreases with reduced growth irradiance as cellular allocation of nitrogen switches away from soluble proteins towards pigment–protein complexes (Hikosaka and Terashima,

© 2010 The Author(s).
This is an Open Access article distributed under the terms of the Creative Commons Attribution Non-Commercial License (http://creativecommons.org/licenses/by-nc/2.5), which permits unrestricted non-commercial use, distribution, and reproduction in any medium, provided the original work is properly cited.

1995; Evans and Poorter, 2001). As a result of these changes, plants grown at low irradiance have a reduced photosynthetic capacity per unit leaf area, yet photosynthetic rates do not differ greatly per unit leaf dry mass. Plants conducting C_4 photosynthesis are generally considered to be less phenotypically plastic with respect to low light acclimation due to their defining anatomical features (Sage and McKown, 2006) although they have also been shown to respond in similar ways to C_3 plants. In an early comparison between the C_4 plant *Zea mays* (maize) and the C_3 plant *Phaseolus vulgaris* (bean), both species had thinner leaves and a lower leaf mass per unit area when grown at lower irradiances (Louwerse and Zweerde, 1977). However, these responses were consistently greater in the C_3 plant, corresponding to a smaller percentage difference in photosynthetic CO_2 assimilation rate between plants grown at high and low irradiance compared with that in the C_4 plant. A study between the sun-adapted C_4 *Z. mays* and the shade-tolerant C_4 grass *Paspalum conjugatum* showed that the response to low irradiance can differ greatly between C_4 plants from different habitats (Ward and Woolhouse, 1986*b*). At low irradiance, the activity of the C_4 photosynthetic enzymes phospho*enol*pyruvate carboxylase (PEPC) and pyruvate P_i dikinase were decreased in both species, yet only in the sun-adapted species did levels of Rubisco, the major component of cellular protein content, fall.

The efficiency of the C_4 photosynthetic concentrating mechanism is intimately linked to bundle sheath leakiness (ϕ) defined as that fraction of CO_2 generated by C_4 acid decarboxylation in the bundle sheath that subsequently leaks out (Farquhar, 1983). Bundle sheath leakiness depends on both the bundle sheath conductance to CO_2 diffusion and the relative biochemical capacities of the C_4 and C_3 cycles, but estimation of these factors remains difficult. Since the C_4 cycle consumes energy in the form of ATP during the regeneration of phospho*enol*pyruvate (PEP), leakage of CO_2 out of the bundle sheath is an energy cost to the leaf. Estimates of leakiness of CO_2 from bundle sheath cells have been shown to increase when measured at lower irradiances (Henderson *et al.*, 1992; Tazoe *et al.*, 2008), contributing to the overall decrease in CO_2 assimilation rate. However, Tazoe *et al.* (2008) also reported that in the C_4 dicot *Amaranthus cruentus*, there was less variation in leakiness in plants grown at low irradiance, suggestive of some acclimation.

The aim of the present study was to measure the response of the C_4 model plant *Flaveria bidentis*, a sun-adapted species, to growth at low irradiance. The potential of a novel 3D growth imaging system to correlate changes in growth with expected physiological, biochemical, and anatomical changes was examined. The specific effects of growth at low irradiance on several factors key to the efficiency of C_4 photosynthesis, namely bundle sheath cell leakiness and both mesophyll and bundle sheath cell conductance to CO_2 diffusion, were also investigated. Concurrent measurements of gas exchange and carbon isotope discrimination are used to estimate bundle sheath leakiness, and anatomical measurements of *F. bidentis* grown at differing irradiances are utilized to estimate mesophyll and bundle sheath conductance to CO_2 diffusion.

Materials and methods

Plant material and growth conditions

Seeds of *F. bidentis* were sown in clear plastic containers measuring 10 cm by 10 cm, and 5 cm in height, containing a commercial seed raising mix (Debco, Melbourne, Australia) and 1 g l^{-1} of a slow release fertilizer (Osmocote, Scotts, Australia). Seeds were germinated in growth cabinets under a 12/12 h day–night cycle at 28/25 °C, 70% humidity at an irradiance of 400 μmol quanta m^{-2} s^{-1}. Following germination, seedlings were transplanted to individual black plastic pots 5 cm by 5 cm, and 10 cm in height containing an identical soil mix and placed in partially water-filled plastic trays. Plants were grown within the same growth cabinet under two light conditions, a medium irradiance of 500 μmol PAR quanta m^{-2} s^{-1} (MI), in which plants were left uncovered, and a low irradiance of 150 μmol PAR quanta m^{-2} s^{-1} (LI), in which plants were continuously covered by a light shade-cloth frame. Forty plants were grown at each irradiance, 15 of which were used for imaging (and subsequent physiological, biochemical, and anatomical measurements) and 25 for destructive harvesting.

Plant imaging and destructive harvesting

Plants were removed from the growth cabinet for imaging every other day for a period of 5–6 weeks. Plants were individually photographed in a Scanalyser growth imaging system (LemnaTec) comprising two cameras to obtain a top view, 0 ° side view, and a 90 ° rotated side view per imaging session. Individual images taken throughout the growth period were used to create and refine an automated analysis algorithm using the Scanalyser software package. The analysis grid was subsequently used to analyse the complete set of images, separating plant from non-plant pixels to give a two-dimensional plant area for each image. Images were calibrated to convert image areas from $pixel^2$ to mm^2. For a single plant the three areas taken at each imaging session were combined to give a plant volume at each time point as shown in Equation 1:

$$PlantVolume = \sqrt[2]{(Area1 \times Area2 \times Area3)} \quad (1)$$

Relative growth rates (RGRs) calculated from image analysis for single plants over the entire growth period were obtained as the slope of an exponential curve fitted to a plot of plant volumes over time. RGRs for dry matter harvests were calculated as in Equation 2:

$$RGR = \frac{Ln^{\mathrm{Mass1}} - Ln^{\mathrm{Mass2}}}{Time1 - Time2} \quad (2)$$

At four time points throughout the growth period (13, 20, 27, and 34 d), 5–10 plants were taken from both light conditions for destructive harvest. Fresh masses of leaves and stems were measured immediately after harvest. Total leaf area (TLA) of each plant was determined using an LI-3000A leaf area meter (LI-COR, Lincoln, NE, USA). Dry masses of leaves and stem were measured after 48 h at 80 °C. Specific leaf area (SLA), leaf dry matter content (LDMC), and leaf dry mass per unit area (LMA) were calculated from destructive harvest data taken from 10 plants after 34 d.

Gas exchange

Gas exchange was measured on the highest fully expanded leaf using a LI-6400 equipped with a blue–red light-emitting diode (LED) light source (LI-COR). Due to the substantial differences in growth rate at different irradiances, plants grown at 500 μmol quanta m^{-2} s^{-1} were measured between 17 d and 30 d after

transplantation of seedlings, whereas plants grown at 150 μmol quanta m^{-2} s^{-1} were measured between 40 d and 50 d after transplantation on an equivalent leaf size and at an equivalent position. Measurements were conducted ~2–3 h into the day cycle. Measured leaves were initially equilibrated for 20 min in a standard environment of 50 μmol mol^{-1} CO_2, 25 °C leaf temperature, flow rate of 500 μmol s^{-1}, and either 150, 500, or 1500 μmol quanta m^{-2} s^{-1} blue–red irradiance depending on the subsequent measurement condition. Photosynthetic CO_2 response (A–C_i) curves were conducted by imposing a stepwise increase in CO_2 partial pressure from 30 μmol mol^{-1} to 600 μmol mol^{-1}, maintaining temperature and irradiance conditions.

Following gas exchange measurements. 0.5 cm^2 leaf discs were removed from the tested leaves and snap-frozen in liquid nitrogen for measurement of photosynthetic enzyme activities and chlorophyll content. The entire opposite leaf was also taken and oven dried at 80 °C for 48 h for later measurement of total nitrogen and carbon isotope composition.

Enzyme activities and chlorophyll measurement

The activities of the photosynthetic enzymes Rubisco and PEPC were measured as previously described by Cousins *et al.* (2007), with some changes. Frozen leaf tissue was processed in ice-cold glass homogenizers with 500 μl of extraction buffer (50 mM HEPES-KOH pH 7.8, 1 mM EDTA, 0.1% Triton-X, 10 mM dithiothreitol, and 1% polyvinylpolypyrrolidone) and 10 μl of protease inhibitor cocktail (Sigma). The homogenate was briefly centrifuged and the supernatant used for assays. For PEPC, 10 μl of leaf extract was combined with 980 μl of assay buffer (50 mM EPPS-NaOH pH 8, 10 mM $MgCl_2$, 0.5 mM EDTA, 0.2 mM NADH, 5 mM glucose-6-phosphate 1 mM $NaHCO_3$, and 1 U ml^{-1} malate dehydrogenase) and the reaction initiated by the addition of 10 μl of 400 mM PEP. For Rubisco, 10 μl of leaf extract was combined with 970 μl of assay buffer (50 mM EPPS-NaOH pH 8, 10 mM $MgCl_2$, 0.5 mM EDTA, 1 mM ATP, 5 mM phosphocreatine, 20 mM $NaHCO_3$, 0.2 mM NADH, 50 U ml^{-1} creatine phosphokinase, 0.2 mg carbonic anhydrase, 50 U ml^{-1} 3-phosphoglycerate kinase, 40 U ml^{-1} glyceraldehyde-3-phosphate dehydrogenase, 113 U m;$^{-1}$ Triose-phosphate isomerase, 39 U ml^{-1} glycerol 3 phosphate dehydrogenase) and the reaction initiated by the addition of 20 μl of 21.9 mM ribulose-1, 5-bisphosphate (RuBP). The activity of both enzymes was calculated by monitoring the decrease of NADH absorbance at 340 nm with a diode array spectrophotometer (Hewlett Packard) after initiation of the reaction.

Chlorophyll was extracted from frozen leaf discs in a glass homogenizer with 80% acetone. The chlorophyll *a* and *b* contents of extracts were measured in a quartz cuvette at 663.3 nm and 646.6 nm, and calculated according to Porra *et al.* (1989).

Leaf anatomical measurements

Multiple leaf pieces of ~2 mm by 5 mm were taken from fully developed source leaves avoiding major veins. Slices were fixed in 5 ml of buffer containing 2.5% gluteraldehyde, 3.5% formaldehyde, 0.1 M Na cacodylate, 0.12 M sucrose, 10 mM ethylene glycol tetra-acetic acid (EGTA), and 2 mM $MgCl_2$ under a vacuum for 4 h. Leaf pieces were subsequently washed in the same buffer lacking fixatives then post-fixed in 1% osmium tetroxide for 2 h. Fixed leaf sections were dehydrated in an ethanol series (50, 60, 70, 75, 80, 90, 95, and 100%) followed by two further rinses in 100% ethanol and two rinses in 100% acetone. Leaf sections were then floated in a 2:1 mix of 100% acetone:araldite resin for 1 h, a 1:1 mix for a further hour, a 1:2 mix for a further hour, followed by three further washes in pure araldite resin for 2 h each. Leaf sections were finally placed in plastic moulds filled with fresh araldite resin and baked at 60 °C for 24 h.

Leaf sections of 0.5 μm thickness were removed from embedded slices using glass knives on an ultramicrotome, stained with toluidine blue, and heat-fixed to glass slides. Slides were viewed using a Zeiss Axioskop light microscope at ×400 magnification. From each slide, three images were produced for analysis, each containing a leaf cross-section in the same orientation, showing at least two vascular bundles. Regions of interest (ROIs) from each cross-section image were selected manually (Fig. 5) using Image J quantification software (NIH, USA).

Calculations of mesophyll surface area exposed to intercellular airspace (S_m) and bundle sheath surface area per unit leaf area (S_b) are given in Equations 3 and 4, respectively. The curvature correction factor (CCF) of 1.43 was taken from Evans *et al.* (1994).

$$S_m = \frac{\text{Length of mesophyll cells exposed to intercellular airspace}}{\text{Interveinal distance}} \times \text{CCF} \quad (3)$$

$$S_b = \frac{\text{Perimeter of bundle sheath tissue within the interveinal distance}}{\text{Interveinal distance}} \quad (4)$$

Leaf vein density analysis

Vein density was measured on leaf sections taken from three plants grown at each irradiance. Leaves were initially cleared by immersion in a 95% ethanol, 5% NaOH solution for 4 d and rehydrated in water for 1 h. Sections were cut from upper, mid, and lower sections of the leaf avoiding major veins, and digital images were taken at ×50 magnification. Vein density was determined from each image by measuring the total length of veins within a 2 cm^2 quadrant using ImageJ quantification software.

Carbon isotope measurements

Plants were transferred from growth cabinets to the laboratory (room temperature 25 °C) and gas exchange measurements were carried out on one fully expanded leaf in the 6 cm^2 leaf chamber of the LI-6400 using a red–blue LED light source (LI-COR). Measured leaves were initially left for 30 min at 25 °C, with an ambient CO_2 of 400 μmol mol^{-1}, an irradiance of 1500 μmol quanta m^{-2} s^{-1}, a flow rate of 200 μmol s^{-1}, and 21% O_2. For subsequent measurements, ambient CO_2 and O_2 were changed to 380 μmol mol^{-1} and 2%, respectively. Gas exchange calculations were adjusted on the LI-6400 program to account for 2% O_2 in the air according to Bunce (2002). Irradiance was adjusted stepwise from 80, to 125, 200, 500, 1500, 1800, 1000, 250, 150, 100, 80, and 0 μmol quanta m^{-2} s^{-1} at 30 min intervals.

The LI-6400 systems were coupled to a tuneable diode laser (TDL; model TGA100, Campbell Scientific, Inc., Logan, UT, USA) for online carbon isotope measurements as described by Bowling *et al.* (2003) and Griffis *et al.* (2004). Input gases (N_2 and O_2) were mixed using mass flow controllers (OMEGA Engineering). Part of the N_2 and O_2 mixture and gas from a compressed air tank were used to correct for gain drift throughout the day. A second calibration gas was created by mixing 10% CO_2 ($\delta^{13}C$= –24.5‰) and part of the N_2/O_2 gas stream in a capillary gas mixing system to generate ~1000 μmol mol^{-1} CO_2. This was then used to generate six different CO_2 concentrations of the same isotopic composition for $^{13}CO_2$ calibration, allowing measurements to be made at different O_2 concentrations. CO_2 cylinders used in the LI-6400 had a carbon isotope composition of 13.1‰ with respect to PDB. The measurement sequence of the TDL consisted of 20 s measurements of zero and six calibration CO_2 concentrations, the compressed air followed by the reference and sample gases of the two LI 6400 machines. The reference gas sampled the inlet gas to the leaf chamber and the sample gases were collected from the tube used to match the infrared gas analysers (IRGAs) in the LI-6400. These gases were dried by

passing through a dryer assembly in the gas line, and $\delta^{13}C$ of the gases was measured by the TDL.

Calculation of CO_2 leakiness

Carbon isotope discrimination (Δ) was calculated using Equation 5 (Evans *et al.*, 1986):

$$\Delta = \frac{\xi(\delta_o - \delta_e)}{1 + \delta_o - \xi(\delta_o - \delta_e)} \quad (5)$$

where δ_e and δ_o are the carbon isotope compositions of dry air entering and leaving the leaf chamber, respectively, measured by the TDL. $\xi = C_e/(C_e - C_o)$, and C_e and C_o are the CO_2 partial pressures of dry air entering and leaving the chamber, respectively, measured by the TDL. CO_2 leakiness (ϕ) was estimated using the model of C_4 carbon isotope discrimination proposed by Farquhar (1983):

$$\Delta = a_b\frac{C_a - C_s}{C_a} + a\frac{C_s - C_i}{C_a} + (e_s + a_l)\frac{C_i - C_m}{C_a} + (b'_4 + (b'_3 - s)\phi)\frac{C_m}{C_a} \quad (6)$$

where C_a, C_s, C_i, and C_m are the CO_2 partial pressures in the air, at the leaf surface, in the intercellular airspace, and in the mesophyll cytoplasm. The symbol a_b is the fractionation during diffusion through the boundary layer (2.9‰), a is the fractionation associated with diffusion of CO_2 in air (4.4‰), e_s is the fractionation during dissolution of CO_2 (1.1‰), a_l is the fractionation during aqueous diffusion (0.7‰), and s is the fractionation during CO_2 leakage from the bundle sheath cells (1.8‰). The combined fractionation of Rubisco, respiration, and photorespiration (b_3') is given by

$$b_3' = b_3 - e(M_m + M_s)/V_c - fV_o/V_c \quad (7)$$

where V_c and V_o are the rates of Rubisco carboxylation and oxygenation, M_m and M_s are the rates of respiration occurring in the mesophyll and bundle sheath cells, respectively, b_3 is the fractionation by Rubisco (30‰), and f is the fractionation associated with photorespiration [11.6‰ (Lanigan *et al.*, 2008)]. The fractionation factor e (–5.1‰) associated with respiration was calculated from the difference between $\delta^{13}C$ in the CO_2 cylinder (–13.1‰) used during experiments and that in the atmosphere under growth conditions (–8‰) (Tazoe *et al.*, 2009).

The combined fractionation of PEP carboxylation, respiration, and fractionation during dissolution of CO_2 and conversion to HCO_3^- is given by

$$b_4' = b_4 + (h - e_b - b_p)V_p/V_h - eM_m/V_p \quad (8)$$

where V_p and V_h are the rates of PEP carboxylation and CO_2 hydration; $b_4 = b_p + e_b + e_s$ (–5.7 ‰ at 25 °C) is the combined fractionation of PEP carboxylation (b_p=2.2‰) and the preceding isotopic equilibrium fractionation (e_b= –9 ‰ at 25 °C) and dissolution of CO_2 (e_s); and h is the fractionation of the catalysed CO_2 hydration (1.1‰). References to the different fractionation factors can be found in Cousins *et al.* (2006) and Henderson *et al.* (1992)

To calculate ϕ, it was assumed that both the boundary layer conductance and the internal conductance to CO_2 diffusion were large ($C_a = C_s$ and $C_i = C_m$) and that there was sufficient carbonic anhydrase activity such that $V_p/V_h = 0$. Since measurements were made at 2% O_2 it was also assumed that $V_o = 0$.

To account for the contribution of respiration in Equations (7) and (8), it was assumed that $M_m + M_s = R_d$, the rate of measured dark respiration, and that $M_m = 0.5R_d$. Using the C_4 photosynthesis model (von Caemmerer, 2000) V_c and V_p were approximated by $V_c = A + R_d$ and $V_p = (A + 0.5R_d)/(1 - \phi)$, respectively, where A is the CO_2 assimilation rate. With these simplifications

$$b_3' = b_3 - e\frac{R_d}{(A - R_d)} \quad (9)$$

and

$$b_4' = b_4 - e\frac{0.5R_d(1 - \phi)}{(A + 0.5R_d)} \quad (10)$$

Using Equations 7–10, Equation 6 can be modified to form:

$$\Delta = a + (e_s + a_l - a)A/(g_m \cdot C_a) + \left[b_4 - e\frac{0.5R_d}{A + 0.5R_d} + \left(b_3 - s - e\left(\frac{R_d}{A + R_d} - \frac{0.5R_d}{A + 0.5R_d}\right)\right)\phi - a\right] \cdot \left(C_i - \frac{A}{g_m}\right)/C_a \quad (11)$$

where g_m is the mesophyll conductance to CO_2 diffusion and $A/g_m = C_i - C_m$.

Rearranging Equation 11 gives an explicit expression of ϕ

$$\phi = \frac{\left(\Delta - a - (e_s + a_l - a)\frac{A}{g_m C_a}\right) - \left(b_4 - e\frac{0.5R_d}{A + 0.5R_d} - a\right)\frac{(C_i - A/g_m)}{C_a}}{\left(b_3 - s - e\left(\frac{R_d}{A + R_d} - \frac{0.5R_d}{A + 0.5R_d}\right)\right)\frac{(C_i - A/g_m)}{C_a}} \quad (12)$$

Note that the inclusion of a finite g_m has only a small effect on the estimates of ϕ.

Dry matter N content and $\delta^{13}C$

Oven-dried leaves were ground to a consistent powder and dried again at 80 °C for 30 min before a small sample was weighed for measurements. The percentage nitrogen was calculated by combustion of samples in an elemental analyser (EA1110, Carlo Erba) and the isotopic composition of CO_2 determined by mass spectrometry. The $\delta^{13}C$ was calculated as $[(R_{sample} - R_{standard})/R_{standard}] \times 1000$, where R_{sample} and $R_{standard}$ are the $^{13}C/^{12}C$ ratio of the sample and the standard V-Pee Dee Belemnite, respectively.

Statistical analysis

The relationship between mean values of photosynthetic, anatomical, and biochemical data obtained throughout this study were tested using the Student's *t*-test ($P < 0.05$). Significant differences are marked with asterisks.

Results

Measurement of growth over 36 days

The growth of *F. bidentis* at LI (150 µmol quanta m^{-2} s) and MI (500 µmol quanta m^{-2} s) was compared using a novel image-based analysis over a 36 d period. Images taken from multiple aspects (see Fig. 1) were combined to give a representative plant volume, allowing the change over time to be measured non-destructively on individual plants. The utility of this approach was that it required a smaller subset of replicated experimental material and allowed individual plants to be measured non-destructively over the entire growth period, thus yielding a large data set sensitive to day-to-day changes in growth. The expected difference in growth between plants grown at the two irradiances was clear in terms of both the plant volume over time (Fig. 2a) and the RGR calculated progressively over time (Fig. 2c.). MI plants grew initially at an RGR of

$\sim$0.24 d^{-1}, declining slightly towards the end of the growth period. Conversely, plants grown at LI began with an RGR of $\sim$0.1 d^{-1}, increasing to $\sim$0.14 d^{-1}. This difference in RGR resulted in a 10-fold difference in plant volumes after 36 d of growth.

To validate the accuracy of this imaging system to measure growth in *F. bidentis*, volume measurements were compared with shoot dry mass (SDM) and TLA measurements made from a series of four destructive harvests of plants (Fig. 2b, d) over the 36 d period. RGRs calculated from TLA (data not shown) and SDM (Fig. 2d) were comparable with RGRs derived from volumes (Fig. 2c). Comparison between TLA and plant volume (Fig. 2e) indicated a similar linear correlation for both groups of plants. A linear correlation was also evident between plant volume and SDM (Fig. 2f) but, at a given volume, plants grown at LI exhibited a lower SDM than those grown at MI.

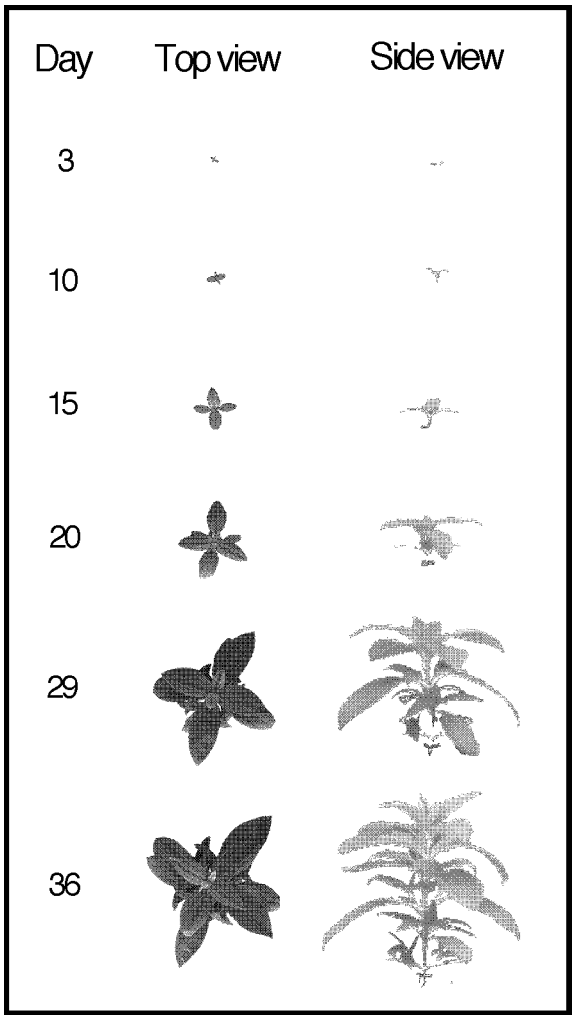

Fig. 1. Top and side images of the *Flaveria bidentis* wild type grown at MI taken over a 36 d period with a 3D growth imaging system (Scanalyser, Lemnatech). Image backgrounds have been removed by the software analysis grid, leaving 2D pictures that are subsequently expressed as a plant area.

SLA, calculated from the destructive harvest of plants grown for 34 d, was significantly higher in plants grown at LI (Table 1). The LDMC and LMA were both higher in plants grown at MI. Furthermore, LI plants allocated 82% of shoot dry matter to leaves compared with 77% in MI plants. Changes in LMA were such that CO_2 assimilation rates measured at high light expressed on a leaf dry mass basis were similar between LI- and MI-grown plants (Table 1).

Photosynthetic CO_2 assimilation

The response of CO_2 assimilation rate (A) to increasing intercellular pCO_2 (C_i) was measured in plants grown at both irradiances using the LI-6400 gas exchange system. To assess photosynthesis under both growth irradiances and at high irradiance, measurements were conducted at a static irradiance of 150, 500, and 1500 μmol quanta m^{-2} s^{-1} at a leaf temperature of 25 °C on all plants. Plants grown at MI had CO_2-saturated assimilation rates of 3.6±0.2, 14.6±0.2, and 31.4±0.4 μmol m^{-2} s^{-1} at these three irradiances, respectively (Fig. 3a). Plants grown at LI had significantly lower CO_2-saturated assimilation rates (Fig. 3c) under 500 μmol quanta m^{-2} s^{-1} and 1500 μmol quanta m^{-2} s^{-1} (12.6±0.2 μmol m^{-2} s^{-1} and 19.3±0.5 μmol m^{-2} s^{-1}, respectively), but slightly higher rates at 150 μmol quanta m^{-2} s^{-1} (4.6±0.1 μmol m^{-2} s^{-1}) than MI plants. MI plants exhibited a steep initial rise in A at low C_i (Fig. 3b) under both 500 μmol quanta m^{-2} s^{-1} and 1500 μmol quanta m^{-2} s^{-1} irradiance. This differed from plants grown at LI (Fig. 3d) where CO_2 assimilation rate increased more slowly at low C_i when measured at 1500 μmol quanta m^{-2} s^{-1} compared with 500 μmol quanta m^{-2} s^{-1}.

Leaf characteristics: enzyme activity, chlorophyll, N, and dry matter $\delta^{13}C$

Rubisco and PEPC activities were measured from leaf disc extracts from plants grown at both irradiances (Table 2). LI plants had 61% lower PEPC activity and 52% lower Rubisco activity, resulting in a lower PEPC/Rubisco ratio. Chlorophyll content per leaf area and chlorophyll *a*/*b* ratio were less in plants grown at LI largely due to a significant difference in chlorophyll *a*. The $\delta^{13}C$ of dried leaf samples was found to be lower in plants grown at LI (–19.8±0.2‰ compared with –16.9±0.1‰). N content per unit leaf area was 18% higher in MI plants (Table 2).

Real-time carbon isotope and CO_2 assimilation rate measurements

Carbon isotope discrimination ($\Delta^{13}C$) and CO_2 assimilation rate (A) were measured in response to real-time changes in irradiance using a system coupling the LI-6400 to a TDL. Measurements were conducted at an ambient CO_2 (C_a) of $\sim$360 μbar with irradiance increasing in steps from 80 μmol quanta m^{-2} s^{-1} to 1800 μmol quanta m^{-2} s^{-1} then decreasing back down. Plants grown at LI had lower CO_2 assimilation rates at higher irradiances compared with

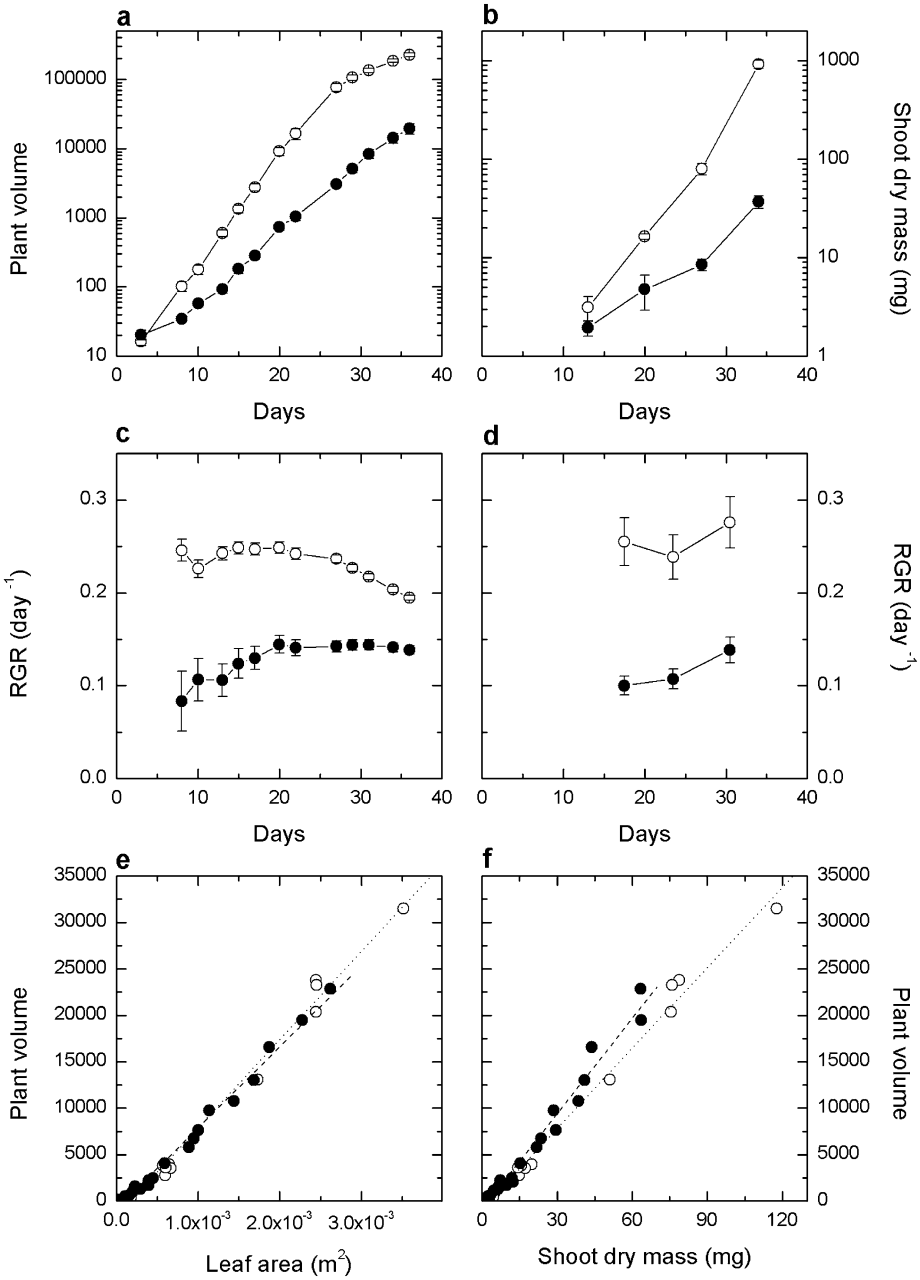

Fig. 2. Comparison between growth measurements derived from image analysis or destructive harvest. Biomass over 36 d using (a) imaging volumes and (b) shoot dry mass. Cumulative relative growth rates from (c) imaging and (d) shoot dry mass. Points indicate the average of 5–10 plants. Correlation between computed volumes from imaging and (e) leaf area and (f) shoot dry mass. Plants grown at an irradiance of 150 μmol quanta m^{-2} s^{-1} (LI) and 500 μmol quanta m^{-2} s^{-1} (MI) are represented by filled and open circles, respectively. In (e) dashed (y=870.77x–803.48) and dotted (y=947.92x–1562.4) lines represent the linear regression for LI and MI irradiance treatments, respectively. In (f) dashed (y=341.91x–850.79) and dotted (y=288.24x–803.47) lines represent the linear regression for LI and MI irradiance treatments, respectively.

plants grown at MI (23.3±1.0 μmol m^{-2} s^{-1} versus 39.9±0.7 μmol m^{-2} s^{-1} at 1800 μmol quanta m^{-2} s^{-1}, Fig. 4a). Stomatal conductance (g_s) increased from low to high irradiance (Fig. 4b) in both sets of plants and was significantly higher in MI plants at any given irradiance. C_i/C_a decreased as irradiance increased, again being greater in MI plants (Fig. 4d). $\Delta^{13}C$ was similar for both groups of plants at >400 μmol quanta m^{-2} s^{-1} (~2‰), yet a greater discrimination was observed in MI plants when measured below 400 μmol quanta m^{-2} s^{-1} (Fig. 4c). Similarly, leakiness (ϕ), calculated using Equation 12, was considerably different between the two groups of plants at low irradiance (Fig. 4e). A measure of uncertainty in $\Delta^{13}C$ (and ϕ) calculations, ξ (Equation 5), remained below 10 at irradiances >400 μmol quanta m^{-2} s^{-1}, yet increased at lower irradiances (Fig. 4f).

Table 1. Leaf properties of *Flaveria bidentis* grown at 150 μmol quanta m^{-2} s^{-1} and 500 μmol quanta m^{-2} s^{-1}

Measurements represent averages and standard errors of 5–10 replicate observations. Asterisks indicate a significant difference in data for plants grown at the differing light intensities.

	Light intensity (μmol quanta m^{-2} s^{-1})	
	150	**500**
A, saturating irradiance (μmol CO_2 m^{-2} s^{-1})	19.3±0.5	31.4±0.4*
A, saturating irradiance (μmol CO_2 g^{-1} s^{-1})	0.92±0.05	0.88±0.04
A, growth irradiance (μmol CO_2 m^{-2} s^{-1})	4.6±0.1	14.6±0.2*
A, growth irradiance (μmol CO_2 g^{-1} s^{-1})	0.22±0.1	0.41±0.08*
SLA leaf area/leaf dry mass (m^2 kg^{-1})	48.2±1.3	28.3±1.0*
LMA leaf dry mass/leaf area (g m^{-2})	20.9±0.6	35.8±1.4*
LAR leaf area/shoot dry mass (m^2 kg^{-1})	39.2±0.9	21.7±1.1*
LDMC leaf dry/fresh mass (mg g^{-1})	91.7±3.0	139.0±5.1*
LDM/SDM leaf dry mass/shoot dry mass (g g^{-1})	0.81±0.01	0.77±0.01*

SLA, specific leaf area; LMA, leaf dry mass per unit area; LAR, leaf area ratio; LDMC, leaf dry matter content; saturating irradiance, 1500 μmol quanta m^{-2} s^{-1}.

Leaf characteristics: anatomy and vein density

The leaf anatomy and vein density of *F. bidentis* plants grown at LI and MI were different in several respects (Table 3). Leaf mesophyll thickness (LMT), as defined in Fig. 5a, was 21% greater in MI than LI plants. As no differences were observed between the average spongy mesophyll or palisade mesophyll cell areas in the two groups of plants, this difference in leaf thickness is partially due to extra mesophyll cell layers rather than an increase in cell size. No significant difference was observed in the width between vascular bundles, defined as the interveinal distance (IVD) in Fig. 5a, although both the bundle sheath cell area and vascular bundle area were higher in plants grown at MI, resulting in larger vascular bodies, as evidenced in Fig. 5b and c. Mesophyll surface area exposed to intercellular airspace (S_m), as defined in Fig. 5a and Equation 3, was substantially higher in MI plants (Table 3). This increase coupled with a small rise in the bundle sheath surface area per unit leaf area (S_b) (due to the increase in size of the vascular tissues and bundle

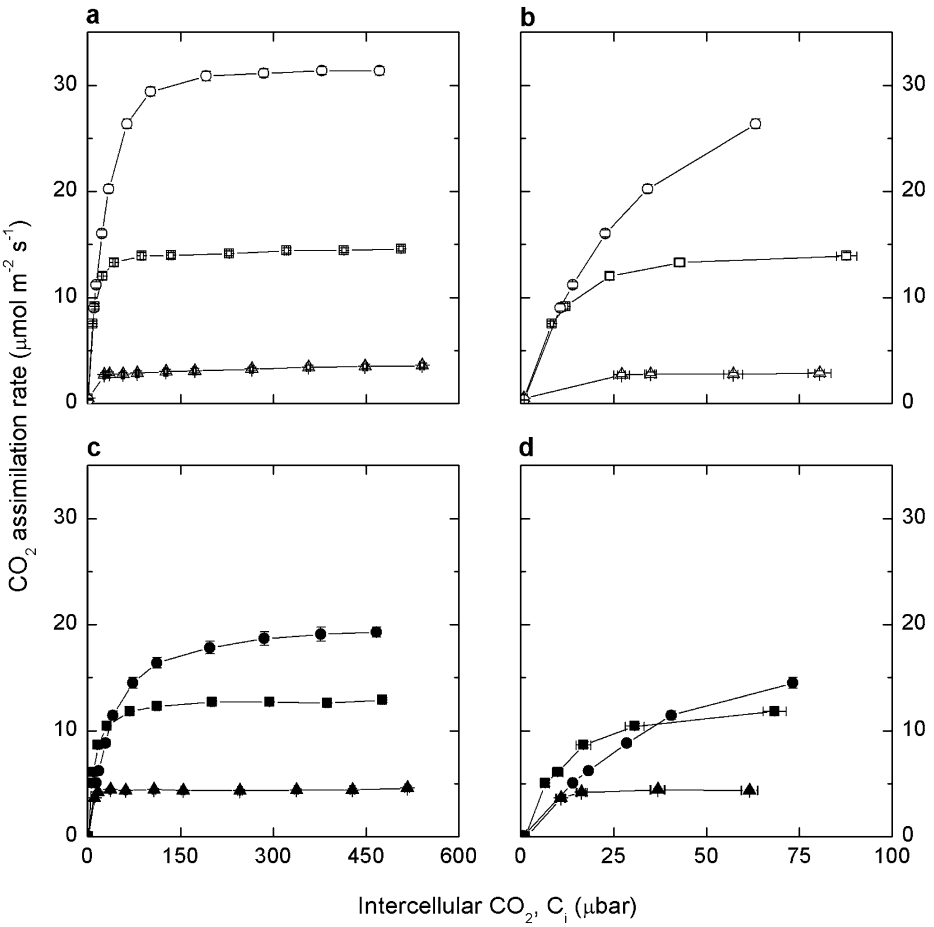

Fig. 3. CO_2 assimilation rate as a function of intercellular pCO_2 (C_i) in *Flaveria bidentis* plants grown at 500 μmol quanta m^{-2} s^{-1} (a, b open symbols) and 150 μmol quanta m^{-2} s^{-1} (c, d filled symbols). Graphs (b) and (d) expand the scale at low C_i to highlight the difference between growth irradiance treatments. Gas exchange measurements were made at three irradiances, 150 (triangle), 500 (square), and 1500 (circle) μmol quanta m^{-2} s^{-1}, and a leaf temperature of 25 °C.

Table 2. Leaf biochemical properties of *Flaveria bidentis* grown at 150 μmol quanta m^{-2} s^{-1} and 500 μmol quanta m^{-2} s^{-1}

Measurements represent averages and standard errors of 5–10 replicate observations. Asterisks indicate a significant difference between plants grown at the two irradiances (P <0.05). Dry matter $\delta^{13}C$ and leaf nitrogen were calculated from destructive harvest measurements of 34-d-old plants.

	Growth irradiance (μmol quanta m^{-2} s^{-1})	
	150	500
PEPC (μmol CO_2 m^{-2} s^{-1})	49.8±4.5	127.0±17.8*
Rubisco (μmol CO_2 m^{-2} s^{-1})	23.9±1.7	50.2±3.3*
PEPC/Rubisco	2.1±0.1	2.5±0.2*
Chlorophyll *a*+*b* (mmol m^{-2})	0.49±0.1	0.63±0.1*
Chlorophyll *a*/*b*	4.7±0.1	5.2±0.1*
Dry matter $\delta^{13}C$ (‰)	–19.8±0.2	–16.9±0.1*
Leaf nitrogen (mmol m^{-2})	77.6±2.0	95.4±5.6*

sheath cells) in MI plants resulted in an increased S_m/S_b. The density of minor tertiary veins was measured in random transects of cleared leaves grown at both irradiances. Although no difference had been found in the IVD measured from leaf cross-sections, vein density was significantly higher in MI plants.

Discussion

The pros and cons of image-based growth analysis

Growth irradiance was used in this study as an easily manipulated stimulus to illustrate the accuracy and effectiveness of an image-based growth analysis in comparison with classical destructive growth measurements. Growth irradiance is known to have considerable effects on growth in C_4 plants, including anatomical, biochemical, and physiological changes to the photosynthetic machinery and operation of the leaves (Ward and Woolhouse, 1986*a*, *b*; Araus *et al.*, 1991; Tazoe *et al.*, 2006). The experimental set-up included 15 plants grown at two irradiances over 34 d, during which imaging was conducted 13 times (Fig. 2a). In contrast, for an equivalent amount of data to be obtained from destructive harvesting, an initial population of 195 plants (at each irradiance) would have been required. In addition to logistical simplification, the imaging approach conferred the singular benefit of being able to match growth data with physiological and anatomical information taken from the same group of plants. Consistent with expectations, differing irradiances during growth produced plants that grew at substantially different rates, resulting in a large difference in final biomass after 36 d (Fig. 2). These growth differences were clearly observed and comparable in measurements made from either imaging or destructive harvest data. RGR is typically calculated from the increase in a plant component mass (leaf, stem, and root) or leaf area over a given time period. Classically, obtaining these biomass data required a destructive harvest in which plants were removed from the soil for measurement, almost unavoidably resulting in plant death (Atkin *et al.*, 1998; Poorter *et al.*, 2005). Less often employed are non-destructive measurement techniques that involve consecutive estimates of plant size through time. This is done through either imaging or painstaking measurement to avoid damaging and thus affecting the growth of plants (Brewster and Barnes, 1981; Weiner *et al.*, 1990). Here, RGR was calculated through imaging, combining three separate images to correct for occlusion of leaves in any one view, giving a representative plant volume. Imaging has previously been used to measure growth in *Arabidopsis thaliana* and *Nicotiana tabacum*, using a single camera mounted above the plants. Leister *et al.* (1999) showed that in *A. thaliana* Col-0, measurement of leaf area using a single top-down image can be significantly affected by overlapping of leaves. Although overlap did not change leaf area estimates in younger plants of this study, in older plants the overlap hid up to 20% of the actual plant area as measured by destructive harvest. Subsequent image-based analyses have avoided this issue by only measuring seedlings early on in the growth period, typically 2–3 weeks after germination (El-Lithy *et al.*, 2004; Walter *et al.*, 2007). As *F. bidentis* seedlings have significant leaf overshadowing, a method was developed that allowed the accurate estimation of leaf area for the first 5 weeks after germination by combining data from a top-view and several side-view images. The plant volumes obtained correlated well with SDM and TLA. It is clear, however, that plant volumes calculated in this manner are not a direct substitute for biomass in situations that change leaf thickness. Linear regression of volume data and destructive data indicates that calculated volumes are still very much an approximated total plant area and do not take into account leaf thickness and thus, if it is reduced, will overestimate plant biomass (Fig. 2f). The estimation of RGR by imaging volumes is not influenced by this overestimation, as it is a relative figure. The technique should therefore be useful for growth analysis of segregating populations of transgenic plants in which replicate samples are not available to facilitate the linking of photosynthetic and growth phenotypes.

Growth response of F. bidentis *to low irradiance*

It has been suggested that C_4 species may be less phenotypically plastic in their growth and photosynthetic response to low light because of the unique anatomical requirements of the C_4 photosynthetic pathway (Sage and McKown, 2006). However *F. bidentis* showed a growth acclimation very similar to that observed in C_3 species (Poorter and van der Werf, 1998). Destructive harvest measurements showed that plants grown at LI were significantly altered in how biomass was invested in leaves as evidenced by an increased LAR relative to plants grown at MI (Table 1) together with a reduced leaf thickness (Table 3). Leaves of *F. bidentis* plants grown at LI were 21% thinner than those grown at MI and had 42% less mass per unit area. In addition, the size of the vascular bundles decreased, as did the average size of the bundle sheath cell surrounding them (Table 3).

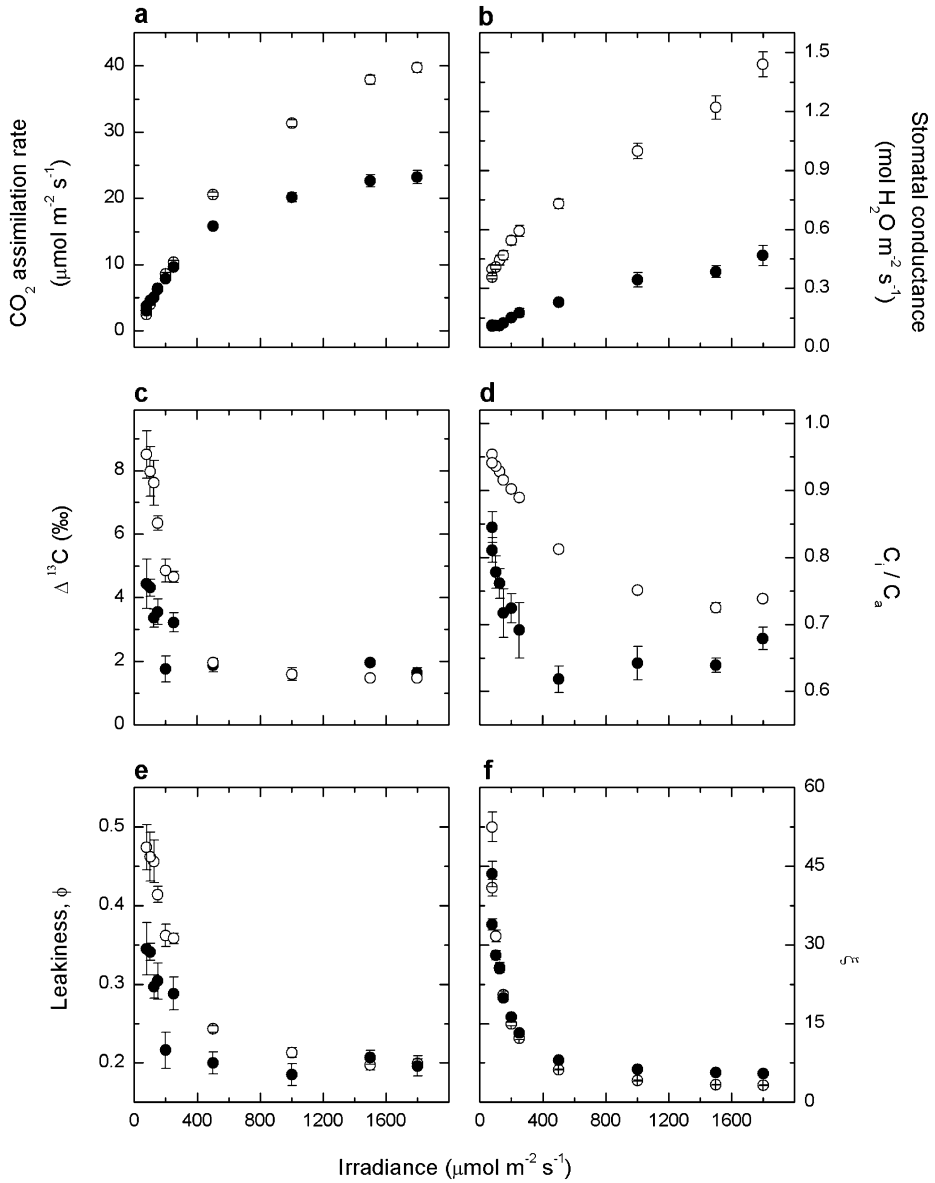

Fig. 4. CO_2 assimilation rate, *A* (a), stomatal conductance, g_s (b), carbon isotope discrimination, Δ (c), the ratio of intercellular to ambient pCO_2, C_i/C_a (d), bundle sheath leakiness, ϕ (e), and ξ (f), as a function of irradiance, in *Flaveria bidentis* grown at 150 μmol quanta m^{-2} s^{-1} (filled circles) and 500 μmol quanta m^{-2} s^{-1} (open circles) irradiance. Measurements were made at an ambient pCO_2 of ~360 μbar, and a leaf temperature of 25 °C.

A decrease in leaf thickness in response to low light intensity has been observed previously in studies on both C_3 and C_4 plants (Louwerse and Zweerde, 1977; Bjorkman, 1981; Ward and Woolhouse, 1986*b*; Araus *et al.*, 1991; Sage and McKown, 2006). This trait has been argued to reduce the construction cost per unit leaf area of any new leaves to match the reduced energy input in a low light environment. As a consequence of the change in SLA, CO_2 assimilation rates at high light were similar in LI and MI plants when expressed per leaf or plant dry mass, which has been commonly observed in C_3 species. At growth irradiance, photosynthetic rates of LI plants were 31% of rates of MI plants on an area basis, but 54% on a mass basis, which was similar to the difference in observed relative growth rates (50–60%, Fig. 2c, d).

Leaf anatomical measurements suggest reduced mesophyll conductance to CO_2 diffusion in F. bidentis *grown at low irradiance*

For photosynthesis to occur, CO_2 has to diffuse from the atmosphere through stomata and intercellular air space into mesophyll cells. Mesophyll conductance (g_m) to CO_2 diffusion has been defined as the conductance to CO_2 diffusion from the intercellular airspace to the chloroplast stroma in C_3 species and to the mesophyll cytosol in C_4 species (Evans and von Caemmerer, 1996). In C_3 species, g_m correlates with the chloroplast surface area appressed to the intercellular air space, and both g_m and chloroplast surface area exposed to the intercellular airspace have been shown to correlate with photosynthetic capacity (von Caemmerer

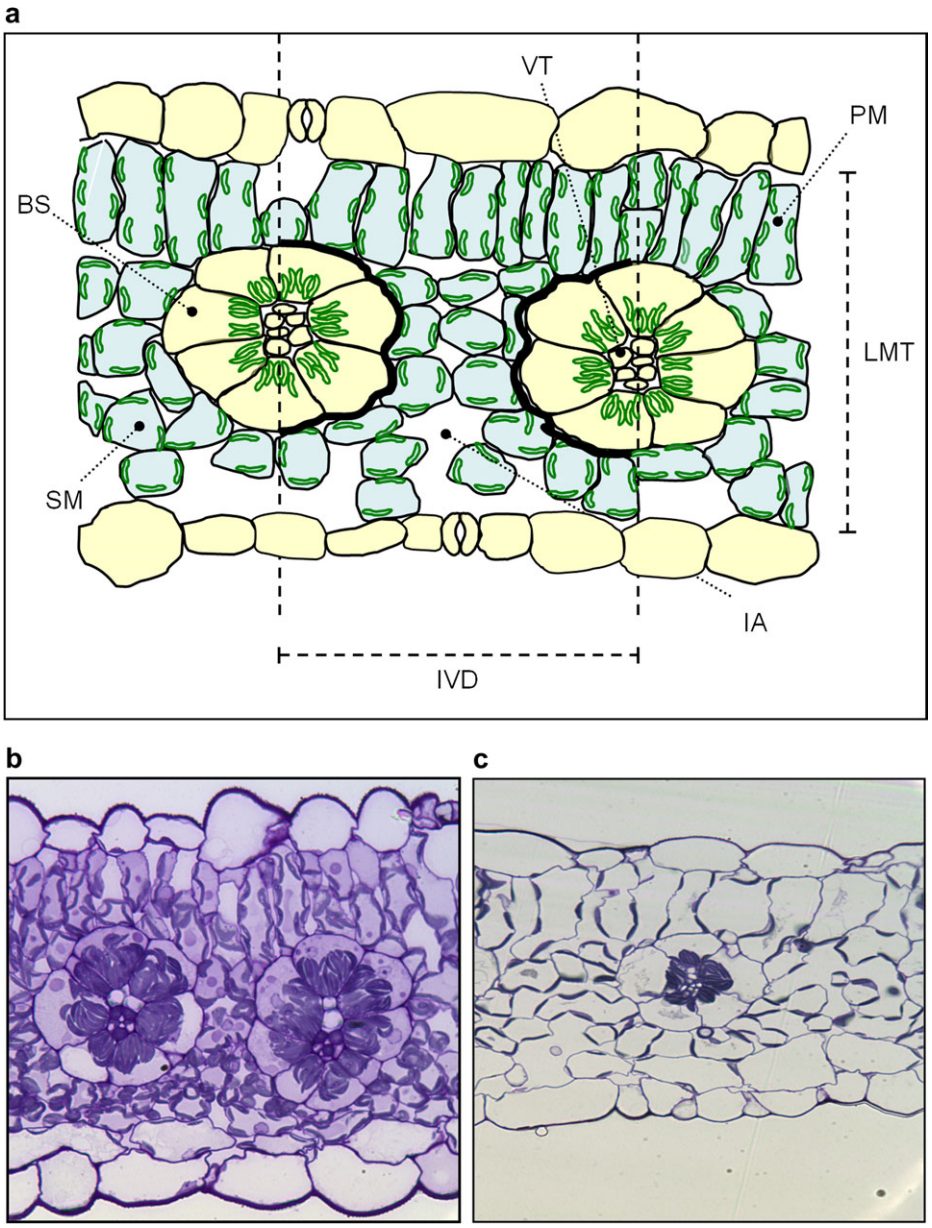

Fig. 5. (a) Diagram representing regions of interest (ROIs) in cross-sections of *Flaveria bidentis* leaves. ROIs include bundle sheath cells (BS), palisade mesophyll cells (PM), spongy mesophyll cells (SM), and total vascular tissue (VT) which were manually outlined and measured to give area and perimeter data. Interveinal distances (IVD) were measured between two adjacent vascular bundles. Leaf mesophyll thickness (LMT) was measured between epidermal layers at four points in each cross-section. Intercellular airspaces (IA) within the interveinal distance were individually outlined and combined to give a total length of mesophyll cells exposed to intercellular airspace (S_m). Black stripes represent the perimeter of the bundle sheath tissue within the interveinal zone (S_b). Representative light microscope images (×400 magnification) of leaf sections of plants grown at 150 μmol quanta m^{-2} s^{-1} (b) and 500 μmol quanta m^{-2} s^{-1} (c).

and Evans, 1991; Evans *et al.*, 2009). C_3 plants grown at low light have lower photosynthetic capacities and lower g_m than high light-grown plants (Hanba *et al.*, 2002; Warren *et al.*, 2007; Yamori *et al.*, 2010). Very little is known about the magnitude of g_m and its variation with photosynthetic capacity in C_4 species since neither carbon isotope discrimination nor fluorescence techniques commonly used to estimate g_m in C_3 species can be used in C_4 species. Because the initial CO_2 fixation occurs in the mesophyll cytosol during C_4 photosynthesis, CO_2 needs only to diffuse across the cell wall, the plasma membrane, and the cytoplasm, and Evans and von Caemmerer (1996) suggested that mesophyll surface area appressed to the intercellular airspace (S_m) would be the relevant parameter to correlate with g_m for C_4 photosynthesis. The present anatomical measurements show that S_m is reduced to a degree similar to photosynthetic capacity (assessed from the CO_2 assimilation rate as measured at high light; Table 3). This suggests that g_m should vary with growth irradiance in C_4 species. Although there is uncertainty in the estimates of the CO_2 permeability for both the cell wall and plasma membrane (Evans *et al.*, 2009), assuming the values of cell wall thickness and

Table 3. Leaf anatomical parameters of *Flaveria bidentis* grown at 150 μmol quanta m^{-2} s^{-1} and 500 μmol quanta m^{-2} s^{-1}

Terminology is defined in Fig. 5a. Parameters represent means and standard errors of 5–20 replicate observations. Asterisks indicate a significant difference between plants grown at the two irradiances (P <0.05).

	Growth irradiance (μmol quanta m^{-2} s^{-1})	
	150	**500**
Leaf mesophyll thickness (μm)	118.7±1.7	150.6±2.1*
Interveinal distance (μm)	139.6±11.2	121.1±7.0
Bundle sheath cell area (μm^2)	402.5±24.5	532.2±14.9*
Palisade mesophyll cell area (μm^2)	446.8±31.2	435.7±18.3
Spongy mesophyll cell area (μm^2)	224.9±9.8	203.9±10.3
Vascular bundle area (μm^2)	175.9±17.2	402.5±31.0*
S_m (m^2 m^{-2})	10.7±0.7	18.0±1.7*
S_b (m^2 m^{-2})	1.7±0.1	2.1±0.1*
S_m/S_b	6.7±0.5	8.8±1.1
Minor vein density (mm mm^{-2})	9.2±0.3	11.2±0.4*

permeabilities used by Evans *et al.* (1994) g_m was estimated to be 0.92 mol m^{-2} s^{-1} bar^{-1} and 0.55 mol m^{-2} s^{-1} bar^{-1} in MI and LI plants, respectively.

Using leaf anatomy to estimate bundle sheath conductance to CO_2 diffusion

The efficiency of the C_4 pathway is dependent upon both the bundle sheath conductance to CO_2 diffusion and the relative biochemical capacities of the C_3 and C_4 cycles. Unfortunately important parameters of the C_4 concentrating mechanism, such as bundle sheath conductance, bundle sheath pCO_2, and leakiness of the bundle sheath, cannot be measured directly, and estimates of bundle sheath conductance vary between 0.01 mol m^{-2} s^{-1} and 0.001 mol m^{-2} s^{-1} (for a review, see von Caemmerer and Furbank, 2003). Bundle sheath conductance expressed on a leaf area basis is dependent on the conductance across the mesophyll–bundle sheath interface and the bundle sheath surface area per unit leaf area (S_b). Estimates of S_b range between 0.6 m^2 m^{-2} and 3.1 m^2 m^{-2}, and the present estimates fall within that range (Apel and Peisker, 1978; Brown and Byrd, 1993).

It is interesting to ask how bundle sheath conductance should vary with changes in photosynthetic capacity observed here under contrasting light environments. Mathematical models of C_4 photosynthesis demonstrated that a low bundle sheath conductance is an essential feature of the C_4 photosynthetic pathway (Berry and Farquhar, 1978; von Caemmerer and Furbank, 1999), and von Caemmerer *et al.* (1997) pointed out that bundle sheath conductance would need to co-vary with biochemical capacity to maintain similar bundle sheath leakiness unless the relative capacities of the C_4 and C_3 cycles also vary. Only a 20% reduction in S_b was observed in LI compared with MI plants, which is less than the 40% reduction observed in CO_2 assimilation rate measured at high irradiance or the reductions observed in Rubisco and PEPC activities (Fig. 3, Tables 1–3).

No differences were observed between LI and MI plants in IVD, a critical parameter in C_4 plants due to the spatial separation of CO_2 fixation processes between mesophyll and bundle sheath cells (Dengler and Nelson, 1999; Ogle, 2003; McKown and Dengler, 2007). However, the smaller bundle sheath cross-sectional area in LI leaves increased separation between the surfaces of the bundle sheath cells and resulted in mesophyll cells that were elongated in the horizontal plane (Fig. 5c). Vein density, which is negatively correlated with IVD amongst *Flaveria* C_3 and C_4 species (McKown and Dengler, 2007), was significantly lower in LI leaves and may more accurately reflect the distance between vascular tissue as it was measured on a larger sample subset. A significant decrease in vein density and increase in IVD was observed in response to lower growth irradiance in the C_4 *Flaveria australasica* (Sage and McKown, 2006). S_b was estimated in two ways: from leaf cross-sections and tracings of bundle sheath perimeters and by combining vein density measurements with estimates of bundle sheath area. The estimates of S_b by the two methods were similar, and reduced vein density as well as reduced bundle sheath area should both contribute to reducing bundle sheath conductance in LI plants.

Anatomical and biochemical acclimation responses to light result in lower bundle sheath leakiness at low irradiance in LI- compared with MI-grown plants

The efficiency of the CO_2-concentrating mechanism is intimately linked to bundle sheath leakiness (ϕ) defined as that fraction of CO_2 generated by C_4 acid decarboxylation in the bundle sheath that subsequently leaks out (Farquhar, 1983). Since the C_4 cycle consumes energy in the form of ATP during the regeneration of PEP, leakage of CO_2 out of the bundle sheath is an energy cost to the leaf particularly pertinent at low light. Both dry matter $\delta^{13}C$ and real-time measurements of $\Delta^{13}C$ were used during gas exchange to assess leakiness in LI and MI plants. As previously reported, lower dry matter $\delta^{13}C$ values were also observed in plants grown at LI, indicative of increased leakiness under low light conditions (Table 1) (Henderson *et al.*, 1992; Cousins *et al.*, 2006; Tazoe *et al.*, 2006). Real-time measurements also showed an increase in leakiness for both LI- and MI-grown plants. Henderson *et al.* (1992) observed comparable results in *Sorghum bicolor* and *Z. mays*, and hypothesized that this increase in leakiness might be due to a change in the coordination of the C_3 and C_4 cycles. Leakiness was similar in LI- and MI-grown plants at irradiances >400 μmol quanta m^{-2} s^{-1} but, at irradiances below this, plants grown at LI maintained a lower leakiness than those grown at MI (Fig. 4). A similar result was reported in the C_4 plant *Amaranthus cruentus* (Tazoe *et al.*, 2008). It is thus noteworthy that reduced vein density did not reduce the efficiency of the C_4 photosynthetic pathway in LI plants. It is possible that the lower bundle sheath conductance in LI-grown plants predicted from the change

in leaf anatomy helped reduce leakiness at low light, but changes in the coordination of the C_3 and C_4 cycle may also be at play. Perhaps at high light the combination of a lower bundle sheath conductance and a lower ratio of PEPC to Rubisco allowed LI plants to maintain a similar leakiness to MI-grown plants, since a lower PEPC to Rubisco ratio lowers bundle sheath CO_2 while a reduced bundle sheath conductance increases bundle sheath CO_2.

The physiological response of *F. bidentis* leaves to growth under low light was very similar to responses observed in C_3 species (Evans, 1988). For example, there was the commonly observed shift to lower chlorophyll *a*/*b* ratios (Table 3) and an increase in SLA (Table 1). When measured at a high irradiance of 1500 μmol quanta m^{-2} s^{-1} the rate of CO_2 assimilation in response to increasing C_i was substantially lower in plants that had been grown at LI compared with MI. This reflected reduced activities of both carboxylating enzymes PEPC and Rubisco measured in LI plants. Interestingly, the initial slope of the CO_2 response curve of the CO_2 assimilation rate was steeper when measured at an irradiance of 500 μmol quanta m^{-2} s^{-1} compared with 1500 μmol quanta m^{-2} s^{-1} in LI plants (Fig. 3d), but the initial slopes were identical in MI plants (Fig. 3b). The initial slope of the curve has been shown in C_4 plants to be limited by PEPC activity (Peisker *et al.*, 1988; Pfeffer and Peisker, 1998), which itself is regulated in part by a reversible light-dependent phosphorylation event (Chollet *et al.*, 1996). This result was unexpected and may again indicate a level of biochemical regulation of PEPC activity achieved by plants grown at LI which contributes to the lower leakiness observed at low light in comparison with MI plants. Further evidence for acclimation is seen under 150 μmol quanta m^{-2} s^{-1} where plants grown at LI reached a significantly higher CO_2 assimilation rate than those grown at MI (Fig. 3a, c).

Conclusion

The growth and photosynthetic response of *F. bidentis* to growth at low light was investigated. Testing a novel three-dimensional imaging system, it was possible to monitor RGRs of individual plants and combine this with leaf physiological analysis. It is concluded that shifts in both leaf anatomy and biochemistry underpin acclimation of growth and photosynthesis to low light in *F. bidentis*, a C_4 dicot. Changes in leaf anatomy predict reduced mesophyll and bundle sheath conductance to CO_2 diffusion in LI plants. Concurrent measurements of gas exchange and carbon isotope analysis show that low light-grown plants are more efficient at low light and achieve lower leakiness under these conditions, suggesting that differences in the coordination of the C_3 and C_4 cycle may be involved.

Acknowledgements

This work was completed with funding from an ARC discovery grant (DP0878395) in both the Research School of Biology at the Australian National University and the Australian Plant Phenomics Facility High Resolution Plant Phenomics Centre, Canberra.

References

Apel P, Peisker M. 1978. Einfluss hoher Sauerstoffkonzentrationen auf den CO_2-Kompensationspunkt von C_4-pflanzen. *Kulturpflanze* **26,** 99–103.

Araus JL, Brown HR, Byrd GT, Serret MD. 1991. Comparative effects of growth irradiance on photosynthesis and leaf anatomy of *Flaveris brownii* (C_4 like), *Flaveria linearis* (C_3–C_4), and their F1 hybrid. *Planta* **183,** 497–504.

Atkin OK, Schortemeyer M, McFarlane N, Evans JR. 1998. Variation in the components of relative growth rate in ten *Acacia* species from contrasting environments. *Plant, Cell and Environment* **21,** 1007–1017.

Berry JA, Farquhar GD. 1978. The CO_2 concentrating function of C_4 photosynthesis: a biochemical model. In: Hall D, Coombs J, Goodwin T, eds. *The Proceedings of the Fourth International Congress on Photosynthesis*. London: Biochemical Society of London, 119–131.

Bjorkman O. 1981. *Responses to different quantum flux densities*. Berlin: Springer-Verlag.

Bowling DA, Sargent SD, Tanner BD, Ehleringer JR. 2003. Tunable diode laser absorption spectroscopy for stable isotope studies of ecosystem–atmosphere CO_2 exchange. *Agricultural and Forest Meteorology* **118,** 1–19.

Brewster JL, Barnes A. 1981. A comparison of relative growth rates of different individual plants and different cultivars of onion of diverse geographic origin at two temperatures and two light intensities. *Journal of Applied Ecology* **18,** 589–604.

Brown RH, Byrd GT. 1993. Estimation of bundle sheath cell conductance in C_4 species and O_2 insensitivity of photosynthesis. *Plant Physiology* **103,** 1183–1188.

Bunce JA. 2002. Sensitivity of infrared water vapor analyzers to oxygen concentration and errors in stomatal conductance. *Photosynthesis Research* **71,** 273–276.

Chollet R, Vidal J, O'Leary MH. 1996. PHOSPHOENOLPYRUVATE CARBOXYLASE: a ubiquitous, highly regulated enzyme in plants. *Annual Review of Plant Physiology and Plant Molecular Biology* **47,** 273–298.

Cousins AB, Badger MR, von Caemmerer S. 2006. Carbonic anhydrase and its influence on carbon isotope discrimination during C_4 photosynthesis. Insights from antisense RNA in *Flaveria bidentis*. *Plant Physiology* **141,** 232–242.

Cousins AB, Baroli I, Badger MR, Ivakov A, Lea PJ, Leegood RC, von Caemmerer S. 2007. The role of phosphoenolpyruvate carboxylase during C_4 photosynthetic isotope exchange and stomatal conductance. *Plant Physiology* **145,** 1006–1017.

Dengler NG, Nelson T. 1999. Leaf structure and development in C_4 plants. In: Sage RF, Monson RK, eds. *C_4 plant biology*. San Diego: Academic Press, 133–172.

El-Lithy ME, Clerkx EJ, Ruys GJ, Koornneef M, Vreugdenhil D. 2004. Quantitative trait locus analysis of growth-related traits in a new *Arabidopsis* recombinant inbred population. *Plant Physiology* **135,** 444–458.

Evans JR, Sharkey TD, Berry JA, Farquhar G. 1986. Carbon isotope discrimination measured concurrently with gas-exchange to investigate CO_2 diffusion in leaves of higher plants. *Australian Journal of Plant Physiology* **13,** 281–292.

Evans JR. 1988. Acclimation by the thylakoid membranes to growth irradiance and the partitioning of nitrogen between soluble and thylakoid proteins. *Australian Journal of Plant Physiology* **15,** 93–106.

Evans JR, Kaldenhoff R, Genty B, Terashima I. 2009. Resistances along the CO_2 diffusion pathway inside leaves. *Journal of Experimental Botany* **60,** 2235–2248.

Evans JR, Poorter H. 2001. Photosynthetic acclimation of plants to growth irradiance: the relative importance of specific leaf area and nitrogen partitioning in maximising carbon gain. *Plant, Cell and Environment* **24,** 755–767.

Evans JR, von Caemmerer S. 1996. Carbon dioxide diffusion inside leaves. *Plant Physiology* **110,** 339–346.

Evans JR, Von Caemmerer S, Setchell BA, Hudson GS. 1994. The relationship between CO_2 transfer conductance and leaf anatomy in transgenic tobacco with a reduced content of Rubisco. *Australian Journal of Plant Physiology* **21,** 475–495.

Farquhar G. 1983. On the nature of carbon isotope discrimination in C_4species. *Australian Journal of Plant Physiology* **10,** 205–226.

Griffis TJ, Baker JM, Sargent SD, Tanner BD, Zhang J. 2004. Measuring field-scale isotopic CO_2 fluxes with tunable diode laser absorption spectroscopy and micrometeorological techniques. *Agricultural and Forest Meteorology* **123,** 15–29.

Hanba YT, Kogami H, Terashima I. 2002. The effect of growth irradiance on leaf anatomy and photosynthesis in *Acer* species differing in light demand. *Plant, Cell and Environment* **25,** 1021–1030.

Henderson SA, Von Caemmerer S, Farquhar GD. 1992. Short-term measurements of carbon isotope discrimination in several C_4 species. *Australian Journal of Plant Physiology* **19,** 263–285.

Hikosaka K, Terashima I. 1995. A model of the acclimation of photosynthesis in the leaves of C_3 plants to sun and shade with respect to nitrogen use. *Plant, Cell and Environment* **18,** 605–618.

Lanigan GJ, Betson N, Griffiths H, Seibt U. 2008. Carbon isotope fractionation during photorespiration and carboxylation in Senecio. *Plant Physiology* **148,** 2013–2020.

Leister D, Varotto C, Pesaresi P, Niwergall A, Salamini F. 1999. Large-scale evaluation of plant growth in *Arabidopsis thalina* by non-invasive image analysis. *Plant Physiology and Biochemistry* **37,** 671–678.

Louwerse W, Zweerde WVD. 1977. Photosynthesis, transpiration and leaf morphology of *Phaseolus vulgaris* and *Zea mays* grown at different irradiances in artificial and sunlight. *Photosymthetica* **11,** 11–21.

McKown AD, Dengler NG. 2007. Key innovations in the evolution of Kranz anatomy and C_4 vein pattern in *Flaveria* (Asteraceae). *American Journal of Botany* **94,** 382–399.

Ogle K. 2003. Implications of interveinal distance for quantum yield in C_4 grasses: a modelling and meta-analysis. *Oecologia* **136,** 532–542.

Peisker M, Apel P, Bauwe H, Pospisilova J, Ticha I. 1988. Relationship between intracellular resistance for CO_2 uptake and phosphoenolpyruvate carboxylase activity in leaves of Zea mays L. *Biochemie und Physiologie der Pflanzen* **183,** 351–354.

Pfeffer M, Peisker M. 1998. CO_2 gas exchange and phosphoenolpyruvate carboxylase activity in leaves of Zea mays L. *Photosynthesis Research* **58,** 281–291.

Poorter H, Perez-Soba M. 2001. The growth response of plants to elevated CO_2 under non-optimal environmental conditions. *Oecologia* **129,** 1–20.

Poorter H, van der Werf A. 1998. Is inherent variation in RGR determined by LAR at low irradiance and NAR at high irradiance? A review of herbaceous species. In: Lambers H, Poorter H, van Vuuren MMI, eds. *Inherent variation in plants growth. Physiological mechanisms and ecological consequences*. Leiden: Backhuys Publishers, 309–336.

Poorter H, van Rijn CP, Vanhala TK, Verhoeven KJ, de Jong YE, Stam P, Lambers H. 2005. A genetic analysis of relative growth rate and underlying components in *Hordeum spontaneum. Oecologia* **142,** 360–377.

Porra RJ, Thompson WA, Kriedmann PE. 1989. Determination of accurate extinction coefficients and simultaneous equations for assaying chlorophyll *a* and *b* extracted with four different solvents: verification of the concentration of chlorophyll standards by atomic absorption spectroscopy. *Biochimica et Biophysica Acta* **975,** 384–394.

Sage RF, McKown AD. 2006. Is C_4 photosynthesis less phenotypically plastic than C_3 photosynthesis? *Journal of Experimental Botany* **57,** 303–317.

Tazoe Y, Hanba YT, Furumoto T, Noguchi K, Terashima I. 2008. Relationships between quantum yield for CO_2 assimilation, activity of key enzymes and CO_2 leakiness in *Amaranthus cruentus*, a C_4 dicot, grown in high or low light. *Plant and Cell Physiology* **49,** 19–29.

Tazoe Y, Noguchi K, Terashima I. 2006. Effects of growth light and nitrogen nutrition on the organization of the photosynthetic apparatus in leaves of a C_4 plant. *Amaranthus cruentus. Plant, Cell and Environment* **29,** 691–700.

Tazoe Y, Von Caemmerer S, Badger M, Evans JR. 2009. Light and CO_2 do not affect the mesophyll conductance to CO_2 diffusion in wheat leaves. *Journal of Experimental Botany* **60,** 2291–2301.

von Caemmerer S. 2000. *Biochemical models of leaf photosynthesis*. Canberra: CSIRO Publishing.

von Caemmerer S, Evans JR. 1991. Determination of the average partial pressure of CO_2 in chloroplast from leaves of several C_3 plants. *Australian Journal of Plant Physiology* **18,** 287–305.

von Caemmerer S, Furbank RT. 1999. Modeling of C_4 photosynthesis. In: Sage RF, Monson R, eds. *C_4 plant biology*. San Diego, CA, USA: Academic Press, 169–207.

von Caemmerer S, Furbank RT. 2003. The C_4 pathway: an efficient CO_2 pump. *Photosynthesis Research* **77,** 191–207.

von Caemmerer S, Millgate A, Farquhar GD, Furbank RT. 1997. Reduction of ribulose-1,5-bisphosphate carboxylase/oxygenase by antisense RNA in the C_4 plant *Flaveria bidentis* leads to reduced

assimilation rates and increased carbon isotope discrimination. *Plant Physiology* **113,** 469–477.

Walter A, Scharr H, Gilmer F, *et al*. 2007. Dynamics of seedling growth acclimation towards altered light conditions can be quantified via GROWSCREEN: a setup and procedure designed for rapid optical phenotyping of different plant species. *New Phytologist* **174,** 447–455.

Ward DA, Woolhouse HW. 1986*a*. Comparative effects of light during growth on photosynthetic properties of NADP-ME type C_4 grasses from open and shaded habitats. II. Photosynthetic enzyme activities and metabolism. *Plant, Cell and Environment* **9,** 271–277.

Ward DA, Woolhouse HW. 1986*b*. Comparative effects of light during growth on photosynthetic properties of NADP-ME type C_4 grasses from open and shaded habitats. I. Gas exchange, leaf anatomy and ultrastructure. *Plant, Cell and Environment* **9,** 261–270.

Warren CR, Low M, Matyssek R, Tausz M. 2007. Internal conductance to CO_2 transfer of adult *Fagus sylvatica*: variation between sun and shade leaves and due to free-air ozone fumigation. *Environmental and Experimental Botany* **59,** 130–138.

Weiner J, Mallory EB, Kennedy C. 1990. Growth and variability in crowded and uncrowded populations of dwarf marigolds (*Tagetes patula*). *Annals of Botany* **65,** 513–524.

Yamori W, Evans JR, Von Caemmerer S. 2010. Effects of growth and measurement light intensities on temperature dependence of CO_2 assimilation rate in tobacco leaves. *Plant, Cell and Environment* **33,** 332–343.